Octupole bands and simplex inversion in the neutron-rich nucleus ^{145}Ba

Yong-Jing Chen (陈永静),[1,*] Zao-Chun Gao (高早春),[1] Yong-Shou Chen (陈永寿),[1] and Ya Tu (图雅)[2]
[1]*Key Laboratory of Science and Technology on Nuclear Data, China Institute of Atomic Energy, Beijing 102413, China*
[2]*College of Physics Science and Technology, Shenyang Normal University, ShenYang 110034, China*
(Received 12 October 2014; revised manuscript received 7 January 2015; published 21 January 2015)

The issue of the existence of reflection asymmetry in ^{145}Ba has stood for the past 30 years without a common conclusion. The recent experimental data show a number of low-lying rotational bands with alternative parities, providing more strict constraints on the relevant modeling. With a proper octupole deformation, all the observed six rotational bands in ^{145}Ba have been well reproduced by the reflection asymmetric shell model (RASM). The three octupole deformed neutron single-particle orbitals just above the octupole shell gap 88, with $K = 1/2$, $K = 3/2$, and $K = 5/2$, respectively, dominate the intrinsic configurations of the observed bands. Based on the analysis of the calculated RASM wave functions, the assignments for the observed bands have been given. The experimental yrast band ($\Delta I = 1$) presents a simplex inversion at around the $11/2^-$ state where the simplex staggering phase changes. This phenomenon may be explained in the framework of the RASM as from the change of the dominate intrinsic configuration, induced by the band mixing. The present results strongly support the appearance of the reflection asymmetry in the ground and low-lying states of ^{145}Ba.

DOI: 10.1103/PhysRevC.91.014317 PACS number(s): 21.60.Cs, 21.10.Re, 27.60.+j

I. INTRODUCTION

Theoretical calculations based on the deformed shell model have predicted the existence of the island of octupole deformed nuclei around $Z = 56$ and $N = 88$ [1,2]. Leander *et al.* [3] predicted that the odd-neutron nucleus ^{145}Ba is a good candidate for octupole deformation. Following the theoretical prediction, several experimental studies, including β-decay [4] and spontaneous fission [5–7], have been made to search for octupole deformation in ^{145}Ba. The first experimental evidence for octupole deformation in ^{145}Ba was reported by Zhu *et al.* in 1999 by measuring the prompt γ rays from spontaneous fission of ^{252}Cf [8]. Five $\Delta I = 2$ rotational bands 1–5, which are built on the $11/2^+$ at 671 keV, the $5/2^-$ ground state, the $7/2^-$ at 112 keV, the $13/2^+$ at 618 keV, and the $19/2^-$ at 1463 keV, respectively, have been established based on the measured linking transition gamma rays. Recently, the excited states in ^{145}Ba, populated in spontaneous fission of ^{248}Cm [9], were reinvestigated by Rzaca-Urban *et al.* [10]. Their results confirm most of the excited levels reported in Ref. [8], and a new band built on the $9/2^-$ at 346 keV was identified, which is denoted as band 6 in the present study. The experimental level scheme of ^{145}Ba employed in the present study is basically the level scheme taken from the ^{252}Cf data [8], and includes an extra band 6 taken from the ^{248}Cm data [10]. These experimental data contain six rotational bands, presenting the most complete spectroscopy for ^{145}Ba to date, and will provide the best constraints for the theoretical models.

^{145}Ba nucleus is predicted to locate at the center of the octupole deformation region [3], however, whether or not the octupole deformation exists in ^{145}Ba is still a controversial topic. For the two neighbor even-even nuclei, ^{144}Ba and ^{146}Ba, the well-established yrast octupole bands have been observed. But the observed yrast band states in ^{145}Ba have not been commonly concluded as the octupole deformed. In Ref. [10], the observed yrast positive and negative bands in ^{145}Ba, the refined ^{248}Cm data, were interpreted as the reflection symmetric states by performing the quasiparticle rotor model (QPRM) calculation with a proper inertial parameter and reasonable Coriolis attenuation factor, and particularly using a reflection symmetric potential. The present study will show that by carrying out the microscopic RASM calculation the yrast and the excited low-lying states observed in ^{145}Ba can be well reproduced and explained as the origin of reflection asymmetry.

Theoretical approaches have been applied to the energy spectra of even-even octupole deformed nuclei around $Z = 56$ and $N = 88$ [11–14]. However, the odd-A nuclei in this region have not been studied sufficiently. In our previous work [15], a precursor analysis of the energy spectra in ^{145}Ba was made with an assumption of the octupole deformation, but only the two observed bands were discussed. A further detailed and complete study for the spectroscopy currently upgraded in ^{145}Ba is necessary to explore the existence of the octupole deformation in the low-lying states of the nucleus. Such a study will also highlight the understanding of the nature of the odd nuclei in the mass region. In the present work, with the starting point of the reflection asymmetric mean field, the reflection asymmetric shell model is applied to describe all the observed six rotational bands in ^{145}Ba.

This paper is organized as follows. Section II presents a brief description of RASM. Calculated results and discussions are presented in Sec. III. A summary is given in Sec. IV.

II. BRIEF DESCRIPTION OF THE THEORY

The reflection asymmetric shell model (RASM) was developed to describe the high spin states in octupole deformed nuclei [16]. In the RASM approach, we first break both the rotational and reflection symmetries in the intrinsic frame, and then carry out simultaneously the angular momentum and

*cyj@ciae.ac.cn

parity projections to make the necessary symmetry restoration in the laboratory frame. The projected states are then used as the basis to diagonalize the spherical shell model Hamitonian. The approach follows the basic philosophy of the standard shell model, and the only difference is that in the RASM the model basis before the projection is deformed rather than the spherical one of the standard shell model. With the projected basis the truncation of the shell model space becomes efficient so that the shell model calculation can be performed for heavy and deformed nuclei, where the traditional shell model has a fateful problem of dimension explosion. We will show that the model space spanned by the states of only three major shells for both protons and neutrons is large enough for the RASM calculation of the low-lying octupole states in the Ba-mass region.

By considering a set of octupole deformed BCS multiquasiparticle states $\{|\Phi_\kappa\rangle\}$ the trial wave function can be constructed as an expansion of the projected states,

$$\left|\Psi_M^{Ip}\right\rangle = \sum_{K\kappa} F_{K\kappa}^{Ip} P_{MK}^{Ip} |\Phi_\kappa\rangle, \tag{1}$$

where $\{P_{MK}^{Ip}|\Phi_\kappa\rangle\} \equiv \{P^p P_{MK}^I|\Phi_\kappa\rangle\}$ is the set of projected multiquasiparticle states with good parity and good angular momentum. P^p and P_{MK}^I are projection operators of parity and angular momentum, respectively,

$$P^p = \frac{1}{2}(1 + p\hat{P}), (p = \pm 1), \tag{2}$$

$$P_{MK}^I = \frac{2I+1}{8\pi^2} \int d\Omega D_{MK}^I(\Omega)\hat{R}(\Omega), \tag{3}$$

where $\hat{P}$ is the parity operator, and p is the parity quantum number. Ω refers to the three Euler angles, $D_{MK}^I(\Omega) = \langle IM|\hat{R}(\Omega)|IK\rangle^*$, and $\hat{R}(\Omega)$ is the rotation operator. The coefficients $F_{K\kappa}^{Ip}$ can be determined by solving the eigenvalue equation,

$$\sum_{K\kappa} \left\{\langle\Phi_{\kappa'}|(H - E^{Ip})P_{K'K}^{Ip}|\Phi_\kappa\rangle\right\} F_{K\kappa}^{Ip} = 0, \tag{4}$$

with the normalization condition,

$$\sum_{K'\kappa'K\kappa} F_{K'\kappa'}^{Ip*} \langle\Phi_{\kappa'}|P_{K'K}^{Ip}|\Phi_\kappa\rangle F_{K\kappa}^{Ip} = 1. \tag{5}$$

Equation (4) is valid for any nuclear shape, but we consider only the case of axial symmetry for the purpose of the present study. The intrinsic states $|\Phi_\kappa\rangle$ in Eq. (1) are the BCS multiquasiparticle states and can be generated by performing the BCS transformation for the deformed single-particle states, where, the κ denotes the quasiparticle (qp) configuration, which include, for the study of highly rotating odd-neutron nuclei, the BCS vacuum $|0\rangle$, the one qp neutron $a_{\mu 1}^\dagger|0\rangle$, the three qp neutrons $a_{\mu 1}^\dagger a_{\mu 2}^\dagger a_{\mu 2}^\dagger|0\rangle$, and three qp one neutron and two protons $a_{\mu 1}^\dagger a_{\pi 1}^\dagger a_{\pi 2}^\dagger|0\rangle$. The deformed single-particle states are obtained with the axial symmetric Nilsson potential which includes the quadrupole, octupole, and hexadecapole deformation terms,

$$\hat{H}_{s.p.} = \hat{H}_0 + \hbar\omega\rho^2\left(-\tfrac{2}{3}\epsilon_2 P_2 + 2\epsilon_3 P_3 + 2\epsilon_4 P_4\right), \tag{6}$$

where $\hat{H}_0$ is the spherical single-particle Nilsson Hamiltonian. $\rho = \sqrt{\frac{m\omega}{\hbar}}r$ is dimensionless, and P_l ($l = 2,3,4$) is the Legendre polynomial. The oscillation frequency is calculated with the standard expression,

$$\hbar\omega = 41A^{-1/3}\left(1 \pm \frac{N-Z}{A}\right)^{1/3} (\text{MeV}), \tag{7}$$

where the $+(-)$ sign stands for neutron (proton). ϵ_2, ϵ_3, and ϵ_4 are the quadrupole, octupole, and hexadecapole deformation parameters, respectively. The quadrupole and hexadecapole couplings between different major shells may be neglected for a simplicity, but the octupole couplings between $\Delta N = 1$ shells must be involved for the description of octupole states.

The RASM Hamiltonian involves a large number of nucleons moving in a spherical Nilsson potential and a interaction of separable multipole $Q \cdot Q$ plus monopole pairing plus quardrupole pairing,

$$\hat{H} = \hat{H}_0 - \frac{1}{2}\sum_{\lambda=2}^{4}\sum_{\tau\tau'} \chi_{\lambda,\tau\tau'} \hat{Q}_{\lambda,\tau} \cdot \hat{Q}_{\lambda,\tau'} - \sum_\tau G_{M,\tau}\hat{P}_\tau \cdot \hat{P}_\tau - \sum_\tau G_{Q,\tau}\hat{P}_{2,\tau} \cdot \hat{P}_{2,\tau}, \tag{8}$$

where τ and τ' refer to neutron or proton, and the second term includes quadrupole ($\lambda = 2$), octupole($\lambda = 3$), and hexadecapole ($\lambda = 4$) interactions, which are responsible for the quadrupole, octupole, and hexadecapole deformations, respectively. The third term represents the monopole pairing with strength G_M, and is the same as the one used in the BCS calculations for self-consistency. The coupling constants, $\chi'_{\lambda,\tau\tau}$ ($\lambda = 2,3,4$), may be determined in the self-consistency with the nuclear deformations by requiring that the HFB vacuum of Eq. (8) (without the quadrupole pairing term) is exactly the BCS vacuum on top of the Nilsson levels from Eq. (6) [16–18]. The quadrupole pairing strength is empirically assumed to be proportional to the monopole pairing strength, and $G_Q = 0.16G_M$ is typically taken.

The Hamiltonian (8) is then diagonalized within the shell model space spanned by the projected states generated from the selected BCS quasiparticle configurations. In the present study only the one-neutron quasiparticle configurations are considered because the one-neutron qp excitations are sufficient to describe the low-lying band states observed in ^{145}Ba except the observed highest spin state in band 5, where the three qp excitation of relevance may play a considerable role in contributing to the moment of inertia. The use of as simple as possible qp configurations in the RASM calculation provides the possibility for achieving a more clear understanding of the underlying physics without the jam of unimportant components.

III. RESULTS AND DISCUSSIONS

A. Projected energy

Unlike the even-even nuclei, the properties of odd-mass nuclei are sensitively affected by the last unpaired nucleon occupying the single-particle orbitals in the vicinity of the Fermi surface. In calculation of the single-particle states

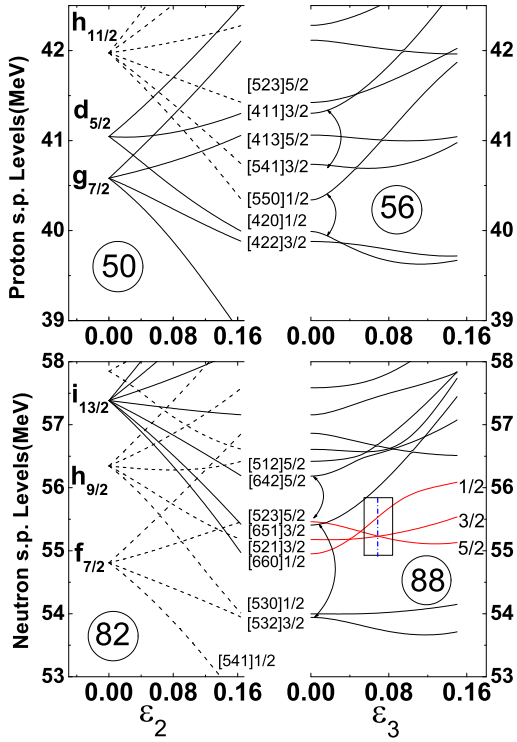

FIG. 1. (Color online) The single proton (upper panel) and neutron (lower panel) levels as a function of quadrupole deformation (ϵ_2) and octupole deformation (ϵ_3). The hexadecapole deformation was involved through $\epsilon_4 = (-0.05/0.168)\epsilon_2$. The adopted orbitals in the present calculations are in red. The vertical dashed line in the box shows the position ($\epsilon_3 \sim 0.07$) of the adopted Nilsson states. The Nilsson parameters (κ,μ) are taken to be (0.090,0.30), (0.065,0.57), and (0.061,0.066) for $N=3$, 4, and 5 proton shells, (0.070,0.39), (0.066,0.33), and (0.063,0.035) for $N=4$, 5, and 6 neutron shells, respectively.

for ^{145}Ba three major shells are included, $N=4,5,6$ for neutrons and $N=3,4,5$ for protons. We plot in Fig. 1 the deformed single-particle states calculated with the Nisson potential. The Nilsson parameters suggested by Bengtsson and Ragnarsson [19] have been taken, but slightly adjusted κ and μ parameters have been adopted for neutrons. It is noticed that this neutron single-particle diagram is similar to the diagram calculated with the Wood-Saxon potential [3]. Around the neutron Fermi surface, three high-j single-particle orbitals, with $K = 1/2$, $K = 3/2$, and $K = 5/2$, present and locate just above the octupole shell gap 88. These orbitals, highlighted with red lines in Fig. 1, will dominate the configurations and consequently determine the properties of the low-lying bands in ^{145}Ba. The octupole shell gaps at proton number 56 and neutron number 88 appear because of the strong octupole correlations between orbitals from the shells (l, j) and $(l-3, j-3)$. Those pairs of octupole coupling orbitals, which are responsible for the octupole deformation of the nucleus, are indicated by arrows in Fig. 1.

In the calculation of the single-particle states the used deformation parameters are $\epsilon_2 = 0.168$ for quadrupole, $\epsilon_3 = 0.067$ for octupole, and $\epsilon_4 = 0.05$ for hexadecapole, which are close

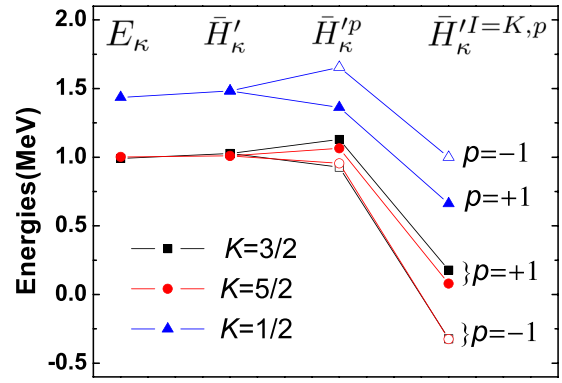

FIG. 2. (Color online) Evolution of the energies for the three selected one-neutron quasiparticle states whose orbitals are shown in Fig. 1. From left to right are the quasiparticle energies E_κ, the expectation values $\bar{H}'_\kappa$ of the Hamiltonian, the parity projected energies $\bar{H}'^{p}_\kappa$, and parity plus angular momentum projected energies $\bar{H}'^{I=K,p}_\kappa$. For the right two columns, the solid (open) symbols stand for the positive (negative) parity states.

to those obtained by the macroscopic-microscopic calculation in Refs. [20,21]. The standard BCS calculation is then performed to obtain the quasiparticle states by using the monopole pairing strength of G/A with $G = 17.14$ MeV for both neutrons and protons. The one-neutron quasiparticle energies, E_κ, for the $K = 1/2$, $K = 3/2$, and $K = 5/2$ configurations are shown in Fig. 2. The $K = 1/2$ quasiparticle energy is considerably higher than the almost degenerated ones for the $K = 3/2$ and $K = 5/2$ configurations. This structure will affect the intrinsic configurations of the rotational bands built on the associated quasiparticle states. We will show that the configuration mixing is strong for the $K = 3/2$ and $K = 5/2$ bands, and a negligible configuration mixing for the $K = 1/2$ band. The expectation values of the Hamiltonian, $\bar{H}'_\kappa = \langle\Phi_\kappa|\hat{H}'|\Phi_\kappa\rangle$ (here, $\hat{H}' = \hat{H} - \lambda\hat{N}$), with respect to the quasiparticle states $|\Phi_\kappa\rangle$ for the $K = 1/2$, $K = 3/2$, and $K = 5/2$ configurations are calculated and shown also in Fig. 2. The $\bar{H}'_\kappa$ values are very close to E_κ, confirming a good self-consistency between the BCS states and the Hamiltonian $\hat{H}$.

The quasiparticle states $|\Phi_\kappa\rangle$ are octupole deformed in the intrinsic frame, and consequently have a mixed parity, no good parity quantum number. Each $|\Phi_\kappa\rangle$ state can be projected into two states $P^p|\Phi_\kappa\rangle$ with $p = \pm 1$, and the corresponding energies can be evaluated through

$$\bar{H}'^{p}_\kappa = \frac{\langle\Phi_\kappa|\hat{H}'P^p|\Phi_\kappa\rangle}{\langle\Phi_\kappa|P^p|\Phi_\kappa\rangle}. \quad (9)$$

The relative energies of the positive and negative parity states, $\bar{H}'^{+}_\kappa$ and $\bar{H}'^{-}_\kappa$, are highly affected by the ratio of the opposite parity components in the state $|\Phi_\kappa\rangle$, and the dominant parity component determines the parity of the lower energy state. As shown in Fig. 2, the $K = 1/2$ state, originated from the $i_{13/2}$ orbital, has a larger positive parity component and, hence, $\bar{H}'^{+}_\kappa$ is lower than $\bar{H}'^{-}_\kappa$. On the contrary, the $K = 3/2$ and $K = 5/2$ states originated from the negative parity shells have a larger negative parity component, and their projected negative parity

states are lower in energy than the corresponding positive parity ones. The energy difference between the projected opposite parity states may be regarded as the parity splitting, which is sensitive to the octupole deformation. The energies of the parity-plus-angular momentum projected states can be calculated by using the expression,

$$\bar{H}_{\kappa}^{\prime Ip} = \frac{\langle \Phi_{\kappa} | \hat{H}^{\prime} P_{KK}^{Ip} | \Phi_{\kappa} \rangle}{\langle \Phi_{\kappa} | P_{KK}^{Ip} | \Phi_{\kappa} \rangle}. \quad (10)$$

For the bandhead states ($I = K$), the energies $\bar{H}_{\kappa}^{\prime I=K,p}$ are calculated and shown again in Fig. 2. Although the angular momentum projection considerably decreases the absolute energies, the parity splitting remains almost unchanged. The energy reduction of the angular momentum projected states reflects the effect of the rotational symmetry restoration in the laboratory frame. The energies of the projected states, $\bar{H}_{\kappa}^{\prime Ip}$, are not ones to be directly compared with the experimental data, however, they contain important information for the band structure in the nucleus. From the calculated energies of $\bar{H}_{\kappa}^{\prime Ip}$ as shown in Fig. 2, it may be expected that for the $K = 1/2$ bands the positive parity band should be lower in energy than the negative parity band, while the ground-state band has the negative parity and the $K = 5/2$ or $K = 3/2$ configuration. Indeed, this feature characterizes the observed low-lying bands in ^{145}Ba.

B. Rotational bands without configuration mixing

The projected energies $\bar{H}_{\kappa}^{\prime Ip}$ with $I \geqslant K$ for each intrinsic state form two rotational bands with opposite parity, which are usually called as "parity doublets." Such calculated rotational bands without configuration mixing are expected to contain the basic nature of the low-lying states in ^{145}Ba because the configuration mixing affects significantly only for a small spin range where the band interaction is strong. Therefore, it is instructive to investigate the low-lying bands with the pure configurations near the Fermi surface. The rotational bands generated by using Eq. (10) for the three selected one-neutron q.p. configurations are shown and compared with the experimental data in Fig. 3. Surprisingly, it is seen that the calculated energies of the band states without the configuration mixing are in nice agreement with the data taken from Refs. [8,10]. This result provides a good guide for the assignments of the observed rotational bands in the nucleus. However, the accurate assignments require the detailed analysis of the corresponding wave functions (see the next section).

The observed positive parity band built on the $13/2^{+}$ level at 618 keV, band 4, as shown in Fig. 3(a), may be assigned as the $K = 1/2$ band based on the [660]1/2 orbital. We notice that this same band was assigned differently as the $K = 3/2$ band based on the [651]3/2 orbital in a previous investigation based on a reflection symmetric potential [10]. Indeed, the [651]3/2 orbital can be considered as the reasonable origin for this excited band because the orbital is near the neutron Fermi surface; see the orbital at $\epsilon_3 = 0$ in Fig. 1. However, the onset of the octupole deformation results in a considerable pushup in energy so that the orbital of relevance becomes far apart from the Fermi level, and, hence, the [651]3/2

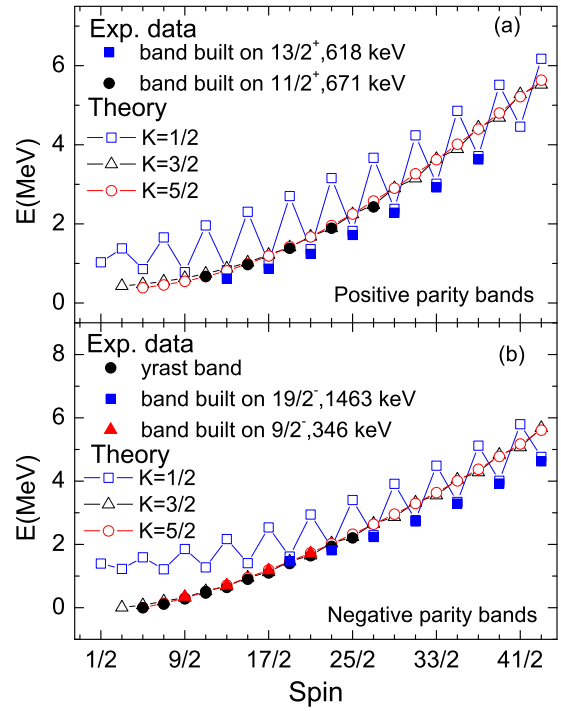

FIG. 3. (Color online) The rotational bands without configuration mixing (open) calculated by using Eq. (10) for the selected one-neutron quasiparticle configurations. The theoretical levels are shifted up by a constant to keep the ground-state energy as zero. The experimental data (solid) are also shown for a comparison. The experimental data are taken from Refs. [8,10].

orbital is no longer optimal for the assignment of the band. Within the context of the RASM, there exists the negative parity $K = 1/2$ band based on the same reflection asymmetric [660]1/2 orbital. The present calculation suggests that the observed negative parity band built on the $19/2^{-}$ level at 1463 keV, band 5 shown in Fig. 3(b), may be based on the [660]1/2 orbital. These two $K = 1/2$ bands have the same simplex quantum number $(+i)$ and opposite parity. Their parity doublet bands with the $K = 1/2$ configuration and the simplex quantum number $(-i)$ are predicted to lie too high in energy to be measured because of the large simplex splitting for the [660]1/2 orbital. This result may explain the missing of such bands in the experimental observations made so far. The previous explanations of the negative parity band built on the $19/2^{-}$ level at 1463 keV have led to a considerable conflict, which was assumed as a possible superdeformed band in Ref. [8] and proposed as an octupole vibrational band coupled to the band 4 in Ref. [10]. The calculated $K = 3/2$ and $K = 5/2$ pure-configuration bands are almost degenerate, implying a strong configuration mixing for the rest of the observed four bands, and, hence, their assignments require the configuration mixing calculation.

C. Rotational bands with configuration mixing

The rotational band energies and the associated wave functions may be calculated by solving the RASM eigenequation, Eq. (4). The calculated rotational bands for ^{145}Ba, the energies

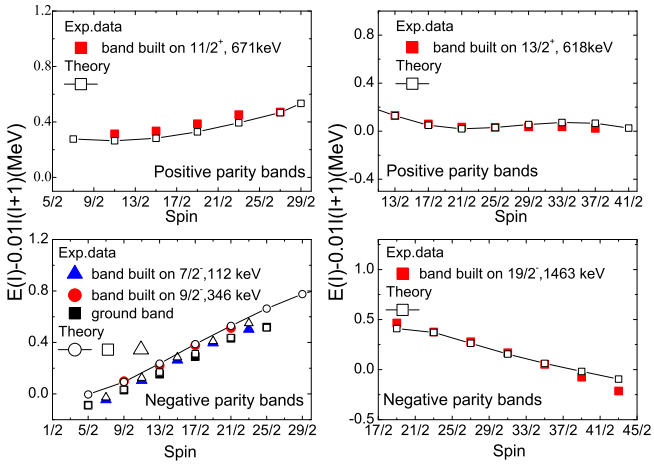

FIG. 4. (Color online) Calculated rotational bands with the configuration mixing (open), and are compared with the experimental data (solid) taken from Refs. [8,10].

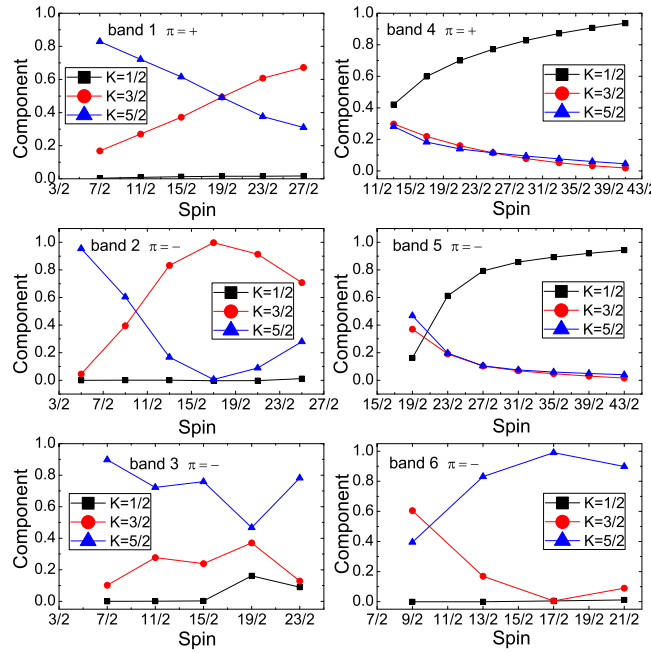

FIG. 5. (Color online) The major components of the $K = 1/2$, $K = 3/2$, and $K = 5/2$ in the wave function corresponding to bands 1–6. $\pi = +$ or $-$ stands for the parity of the rotational band.

as a function of spin, are compared with the experimental data and shown in Fig. 4. A good agreement between theory and experiment was achieved not only for the yrast bands but also for all the observed excited bands. The complex spectroscopic data for ^{145}Ba are characterized by the fact that the alternative parity bands appear in a very low-energy range, presenting theoretical challenges. To reproduce all the observed rotational bands in ^{145}Ba, we found that the inclusion of the octupole degree of freedom in the theory is essential. The QPRM calculations are based on an axial and reflection symmetric nuclear potential reproduced the observed positive parity band built on the $13/2^+$ at 618 keV, but only a poor agreement between theory and experiment was achieved for the negative parity ground-state band, as shown in Fig. 12 of Ref. [10]. In contrast, the present RASM calculations with a proper octupole deformation have well reproduced the experimental data that contain six observed rotational bands in ^{145}Ba, implying the occurrence of the reflection asymmetric shape in this neutron-rich nucleus.

The wave functions of the low-lying states obtained by solving Eq. (4) are dominated by the $K = 1/2$, $K = 3/2$, and $K = 5/2$ configurations, based on the neutron [660]1/2, [521]3/2, and [523]5/2 orbitals, respectively. The components of the wave functions may be calculated through the expression,

$$A_\kappa(Ip) = \sum_{K'\kappa', K} F^{Ip*}_{K'\kappa'} \langle \Phi_{\kappa'} | P^{Ip}_{K'K} | \Phi_\kappa \rangle F^{Ip}_{K\kappa}, \qquad (11)$$

with $\sum_\kappa A_\kappa(Ip) = 1$ according to Eq. (5). The $A_\kappa(Ip)$ for the three lowest quasiparticle configurations are calculated and shown in Fig. 5. The $K = 1/2$ quasiparticle energy is quite larger than the $K = 3/2$ and $K = 5/2$ energies, but the last two are very closed to each other even after the projections, as shown in Fig. 2. It is then expected that a somewhat pure configuration presents in the $K = 1/2$ bands, and a strong configuration mixing occurs in the $K = 3/2$ and $K = 5/2$ bands. In band 1, built on the $11/2^+$ level at 671 keV, the $K = 5/2$ component dominates the wave function at low spins and decreases with increasing spin, while the $K = 3/2$ component increases with increasing spin and becomes the major one at spin 27/2. In band 2, built on the $5/2^-$ ground state, the $K = 5/2$ component dominates the wave function at the bandhead but decreases so quickly with spin that the $K = 3/2$ component dominates the wave function at $I \geqslant 13/2$. In band 3, built on the $7/2^-$ state at 112 keV, the $K = 5/2$ component dominates the wave function at the entire spin range except a considerable large mixing occurs at spin 19/2. In band 6, built on the $9/2^-$ state at 346 keV, the $K = 3/2$ and $K = 5/2$ components are comparable at the bandhead, and the latter becomes dominant at $I \geqslant 13/2$. In band 4 and band 5, built on the $13/2^+$ state at 618 keV and the $19/2^-$ state at 1463 keV, respectively, the $K = 1/2$ component dominates the wave function within almost the entire spin range, and the $K = 3/2$ and $K = 5/2$ components compete with the $K = 1/2$ one only at the bandheads. The $K = 3/2$ and $K = 5/2$ configurations present a strong mixing in a number of bands, and, hence, the configuration assignment encounters some difficulties. By considering the configuration mixing at the bandhead and complementing the mixing in the entire band, the analysis of the RASM wave functions, as presented in Fig. 4, suggests the assignment of the $K = 5/2$ configuration for band 1, band 3, and band 6, and the assignment of the $K = 1/2$ for band 4 and band 5. For band 2, the $K = 3/2$ configuration may be assigned in terms of the main component in the large spin range, or assigned alternatively as the $K = 5/2$ band in terms of the dominate component at the bandhead.

For the quadrupolely deformed system the symmetry under $\hat{R}_x(\pi)$ and the associated "signature" quantum number r, have been often used in the nuclear spectroscopy studies.

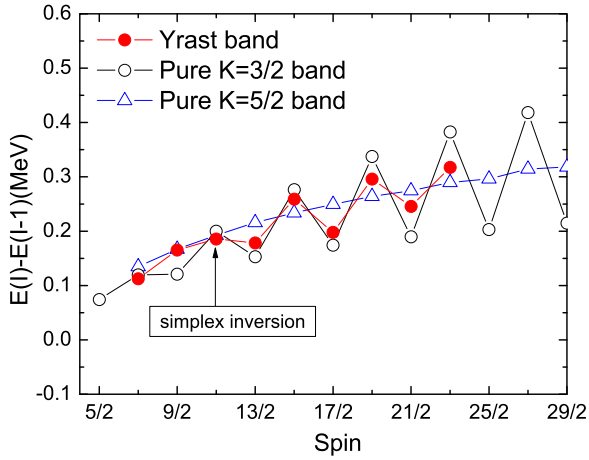

FIG. 6. (Color online) The difference energies $E(I) - E(I-1)$ for the experimental yrast band ($\Delta I = 1$) (solid) and for the calculated bands ($\Delta I = 1$) with the pure configurations of $K = 3/2$ and $K = 5/2$. The simplex inversion presents at around spin 11/2.

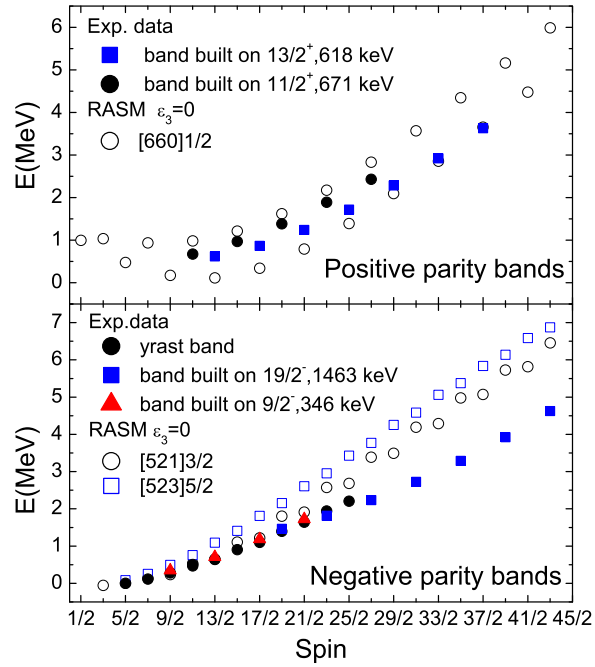

FIG. 7. (Color online) Theoretical rotational bands (open), calculated with $\epsilon_3 = 0$, and keeping other parameters being unchanged, are compared with the experimental data (solid).

This quantum number cannot be used in the description of the reflection asymmetric system. The symmetry under $\hat{S} = \hat{\pi}\hat{R}_x^{-1}(\pi)$, where $\hat{\pi}$ denotes the intrinsic parity operator, and the associated "simplex" quantum number s, have been applied to the octupole deformed nuclei [22]. Within this classification scheme the octupole deformed states can be labeled in terms of parity and simplex (π,s). In an odd-even octupole deformed nucleus, like ^{145}Ba, the simplex $s = +i$ classifies the states with spin and parity of $J^\pi = 1/2^+,3/2^-,5/2^+,7/2^-,\ldots$, while the simplex $s = -i$ labels the states of $J^\pi = 1/2^-,3/2^+,5/2^-,7/2^+,\ldots$. In the context of the RASM, the observed six rotational bands in ^{145}Ba are described as the octupole bands and can be classified with the quantum numbers (π,s), e.g., $(-,-i)$ for band 2 and $(-,+i)$ for band 3. The yrast band ($\Delta I = 1$) has the negative parity and contains two ($\Delta I = 2$) sequences with opposite simplex, namely, band 2 and band 3. The energy splitting defined to be the difference of $E(I) - E(I-1)$ in the ($\Delta I = 1$) band may be regarded as the simplex splitting. In the yrast band of ^{145}Ba, the observed simplex splitting presents the energy staggering and the staggering phase changes at around spin 11/2, as shown in Fig. 6, and this phenomenon may be called the simplex inversion. The simplex splitting and the simplex inversion observed in the yrast band was well reproduced by the present calculation, and the underlying physics may be understood through the analysis of the calculated RASM wave functions. The calculated component distribution is very different for band 2 and band 3, as shown in Fig. 5. The dominant configuration in band 2 changes dramatically from the $K = 5/2$ to the $K = 3/2$ at spin 11/2, while the dominant component in band 3 is the $K = 5/2$ at low spins and presents a graduate reduction for the states of $I \geqslant 11/2$. Consequently, in the yrast band the spin 11/2 becomes a critical point whereafter the major configuration $K = 5/2$ changes to the $K = 3/2$, causing the change of the simplex staggering phase. We also note that the simplex splitting behaves very differently for the pure $K = 5/2$ band than the pure $K = 3/2$ band, as shown in Fig. 6. The pure $K = 3/2$ band has a much larger simplex splitting and a different simplex staggering phase at low spins in comparison with the pure $K = 5/2$ band. Therefore, the simplex inversion occurs once the major configuration changes from $K = 5/2$ to $K = 3/2$. This is an interpretation of the simplex inversion suggested by the present RASM calculation. The simplex inversion phenomenon is expected to occur in other octupole deformed nuclei, e.g., in the neighbor nucleus ^{141}Ba, because the band mixing, being the phenomenon driven factor, is a common effect of the Coriolis force.

Figure 7 shows the low-lying rotational bands calculated with $\epsilon_3 = 0$ but keeping other parameters being unchanged in the attempt to demonstrate the fatal difficulty of reproducing the experimental spectroscopic data without considering a proper octupole deformation. The calculated yrast band ($\Delta I = 1$) becomes to the $K = 3/2$ negative parity one, differing from the experimental $K = 5/2$ negative parity yrast band, and the calculated energies of the yrast states are consistent with the experimental data only within a short range of spin, $I \leqslant 13/2$. The upper part of the yrast band and in particular all the observed side bands ($\Delta I = 2$), the two negative parity bans and two positive parity bands, are not reproduced at all, as shown in Fig. 7. In fact, the similar situation was encountered for the calculation by using the reflection symmetric particle rotor model in Ref. [10], where only one observed band in ^{145}Ba can be reproduced reasonably well. It is therefore important to invoke the octupole asymmetry for the description of the complex alternative parity rotational low-lying bands observed in ^{145}Ba.

IV. SUMMARY

Recently, the spectroscopic data for the neutron-rich nucleus ^{145}Ba has reached a new level of both quality and completeness and provide more strict constrains on the modeling of the reflation asymmetry. The reflection asymmetric shell model (RASM) calculation was performed to investigate the reflection asymmetry in ^{145}Ba. All the observed six rotational bands are well reproduced by the present calculation with a proper octupole deformation of $\epsilon_3 \sim 0.07$, which is consistent with the macroscopic-microscopic calculations in the literature, and the assignments of these low-lying bands in terms of the parity and simplex (π,s) and the intrinsic configuration have been given. Three octupole deformed Nilsson orbitals, namely, the neutron [521]3/2, [523]5/2, and [660]1/2, located just above the octupole shell gap 88, are found to dominate the intrinsic structure of the observed low-lying states. The calculated results show that the positive parity band ($\Delta I = 2$) built on the $13/2^+$ level at 618 keV and the negative parity band built on the $19/2^-$ level at 1463 keV are based on the [660]1/2 orbital, and may be assigned with $K = 1/2$ and simplex $s = +i$. The $5/2^-$ ground-state band and the positive parity band built on the $11/2^+$ level at 671 keV are identified as the simplex $s = -i$ parity-partner bands based on the $K = 5/2$, [523]5/2 orbital mixed with the $K = 3/2$, [521]3/2 state. The energies of the $K = 3/2$ and $K = 5/2$ quasiparticles are very close to each other so that the configuration mixing is strong for the bands based on these two orbitals. In contrast, the bands based on the the $K = 1/2$ orbital have a quite pure configuration as the quasiparticle energy is considerably higher than the $K = 3/2$ and $K = 5/2$ quasiparticles. The simplex splitting and the simplex inversion observed in the yrast band ($\Delta = 1$) have been well reproduced by the present calculation, and the simplex inversion phenomenon can be interpreted as from the strong mixing between the $K = 3/2$ and $K = 5/2$ configurations in the RASM wave functions. The present study strongly supports the appearance of the reflection asymmetric shape in the ground and low-lying states of ^{145}Ba. The future experimental discoveries of the octupole bands, which are predicted by the present calculation but have not yet been measured, will certainly confirm this conclusion.

ACKNOWLEDGMENTS

We thank Professor S. J. Zhu for the stimulating discussions and his confirmation for the experimental data employed in the present study. The work was supported by the National Natural Science Foundation of China under Grants No. 11205246, No. 11321064, No. 11175258, No. 11305108, and No. 11275068.

[1] W. Nazarewicz, P. Olanders, I. Ragnarsson, J. Dudek, G. A. Leander, P. Moller, and E. Ruchowska, Nucl. Phys. A **429**, 269 (1984).
[2] W. Nazarewicz and P. Olanders, Nucl. Phys. A **441**, 420 (1985).
[3] G. A. Leander, W. Nazarewicz, P. Olanders, I. Ragnarsson, and J. Dudek, Phys. Lett. B **152**, 284 (1985).
[4] J. D. Robertson, S. H. Faller, W. B. Walters, R. L. Gill, H. Mach, A. Piotrowski, E. F. Zganjar, H. Dejbakhsh, and R. F. Petry, Phys. Rev. C **34**, 1012 (1986).
[5] S. J. Zhu, Q. H. Lu, J. H. Hamilton, A. V. Ramayya, L. K. Peker, M. G. Wang, W. C. Ma, B. R. S. Babu, T. N. Ginter, J. Kormicki, D. Shi, J. K. Deng, W. Nazarewicz, J. O. Rasmussen, M. A. Stoyer, S. Y. Chu, K. E. Gregorich, M. F. Mohar, S. Asztalos, S. G. Prussin, J. D. Cole, R. Aryaeinejad, Y. K. Dardenne, M. Drigert, K. J. Moody, R. W. Loughed, J. F. Wild, N. R. Johnson, I. Y. Lee, F. K. McGowan, G. M. Ter-Akopian, and Yu. Ts. Oganessian, Phys. Lett. B **357**, 273 (1995).
[6] M. A. Jones, W. Urban, J. L. Durell, M. Leddy, W. R. Phillips, A. G. Smith, B. J. Varley, I. Ahmad, L. R. Morss, M. Bentaleb, E. Lubkiewicz, and N. Schulz, Nucl. Phys. A **605**, 133 (1996).
[7] J. H. Hamilton, A. V. Ramayya, J. K. Hwang, J. Kormick, B. R. S. Babu, A. Sandulescu, A. Florescu, W. Greiner, G. M. Ter-Akopian, Yu. Ts. Oganessian, A. V. Daniel, S. J. Zhu, M. G. Wang, T. Ginter, J. K. Deng, W. C. Ma, G. S. Popeko, Q. H. Lu, E. Jones, R. Dodder, P. Gore, W. Nazarewicz, J. O. Rasmussen, S. Asztalos, I. Y. Lee, S. Y. Chu, K. E. Gregorich, A. O. Macchiavelli, M. F. Mohar, S. Prussin, M. A. Stoyer, R. W. Lougheed, K. J. Moody, J. F. Wild, A. Bernstein, J. A. Becker, J. D. Cole, R. Aryaneinejad, Y. X. Dardenne, M. W. Drigert, K. Butler-moore, R. Donangelo, and H. C. Griffin, Prog. Part. Nucl. Phys. **38**, 273 (1997).
[8] S. J. Zhu, J. H. Hamilton, A. V. Ramayya, E. F. Jones, J. K. Hwang, M. G. Wang, X. Q. Zhang, P. M. Gore, L. K. Peker, G. Drafta, B. R. S. Babu, W. C. Ma, G. L. Long, L. Y. Zhu, C. Y. Gan, L. M. Yang, M. Sakhaee, M. Li, J. K. Deng, T. N. Ginter, C. J. Beyer, J. Kormicki, J. D. Cole, R. Aryaeinejad, M. W. Drigert, J. O. Rasmussen, S. Asztalos, I. Y. Lee, A. O. Macchiavelli, S. Y. Chu, K. E. Gregorich, M. F. Mohar, G. M. Ter-Akopian, A. V. Daniel, Yu. Ts. Oganessian, R. Donangelo, M. A. Stoyer, R. W. Lougheed, K. J. Moody, J. F. Wild, S. G. Prussin, J. Kliman, and H. C. Griffin, Phys. Rev. C **60**, 051304 (1999).
[9] P. J. Nolan, F. A. Beck, and D. B. Fossan, Annu. Rev. Nucl. Part. Sci. **44**, 561 (1994).
[10] T. Rzaca-Urban, W. Urban, J. A. Pinston, G. S. Simpson, A. G. Smith, and I. Ahmad, Phys. Rev. C **86**, 044324 (2012).
[11] J. L. Egido and L. M. Robledo, Nucl. Phys. A **545**, 589 (1992).
[12] Y. X. Liu, H. Z. Sun, and E. G. Zhao, J. Phys. G **20**, 1771 (1994).
[13] E. Garrote, J. L. Egido, and L. M. Robledo, Phys. Lett. B **410**, 86 (1997).
[14] A. R. H. Subber and Falih H. Al-Khudair, Phys. Scr. **84**, 035201 (2011).
[15] Chen Yong-Jing, Chen Yong-Shou, Zhu Sheng-Jiang, Gao Zao-Chun, and Tu Ya, Chin. Phys. Lett. **22**, 1362 (2005).
[16] Y. S. Chen and Z. C. Gao, Phys. Rev. C **63**, 014314 (2000).
[17] K. Hara and Y Sun, Int. J. Mod. Phys. **E4**, 637 (1995).
[18] P. Ring and P. Schuck, *The Nuclear Many-Body Problem* (Springer, New York, 1980).
[19] R. Bengtsson and I. Ragnarsson, Nucl. Phys. A **415**, 189 (1984).
[20] P. Muller, J. R. Nix, W. D. Myers, and W. J. Swiatecki, Atomic Data and Nuclear Data Tables **59**, 185 (1995).
[21] P. Muller, R. Bengtsson, B. G. Carlsson, P. Olivius, T. Ichikawa, H. Sagawa, and A. Iwamoto, Atomic Data and Nuclear Data Tables **94**, 758 (2008).
[22] W. Nazarewicz, P. Olanders, I. Ragnarsson, J. Dudek, and G. A. Leander, Phys. Rev. Lett. **52**, 1272 (1984).